

Optimal thermoelectricity with quantum spin-Hall edge states

Daniel Gresta,¹ Mariano Real,² and Liliana Arrachea¹

¹*International Center for Advanced Studies, ECyT-UNSAM,
Campus Miguelete, 25 de Mayo y Francia, 1650 Buenos Aires, Argentina*

²*Instituto Nacional de Tecnología Industrial, INTI,
Av. General Paz 5445, (1650) Buenos Aires, Argentina*

We study the thermoelectric properties of a Kramer's pair of helical edge states of the quantum spin Hall effect coupled to a nanomagnet with a component of the magnetization perpendicular to the direction of the spin-orbit interaction of the host. We show that the transmission function of this structure has the desired qualities for optimal thermoelectric performance in the quantum coherent regime. For a single magnetic domain there is a power generation close to the optimal bound. In a configuration with two magnetic domains with different orientations, pronounced peaks in the transmission functions and resonances lead to a high figure of merit. We provide estimates for the fabrication of this device with HgTe quantum-well topological insulators.

Introduction. Thermoelectricity in the quantum regime is attracting high interest for some years now [1, 2]. Systems hosting edge states, like the quantum Hall and quantum spin Hall are paradigmatic realizations of quantum coherent transport. Several theoretical and experimental results on heat transport and thermoelectricity in these systems have been recently reported [3–30].

Unlike the quantum Hall state, which is generated by a strong magnetic field, the quantum spin Hall (QSH) state taking place in two-dimensional (2D) topological insulators (TI), preserves time-reversal invariance. Therefore, the edge states appear in helical Kramer's pairs [31–36] with opposite spin orientations determined by the spin orbit of the TI. Several heat engines and refrigerators have been recently proposed, taking advantage of the fundamental chiral nature of the quantum Hall edge states, which manifests itself in multiple-terminal structures [19] and in quantum interference [20]. Recently, the property of charge fractionalization was also pointed out as a mechanism to enhance thermoelectricity [22]. All these setups rely on the existence of quantum point contacts and quantum dots in the structure, tunnel-coupled to the edge states, which are generated by recourse to constrictions. The fabrication of these elements is nowadays normal in the context of the quantum Hall effect [37–39]. However, their realization in the context of the QSH effect remains an experimental challenge so far, although they are widely investigated theoretically [40–49].

In the quantum coherent regime the electronic transport properties take place without inelastic scattering and are fully characterized by the transmission function. Particle-hole symmetry breaking is a necessary condition for steady-state heat to work conversion. Hence, having transmission functions rapidly changing in energy within the relevant transport window, is the key to achieve optimal thermoelectricity [2, 50–53]. The optimal performance is usually quantified by the *figure of merit* ZT , with the Carnot limit achieved for $ZT \rightarrow \infty$. This ideal limit can be realized for transmission functions containing delta-function like peaks [50]. In this sense, structures with resonant levels like quantum dots are partic-

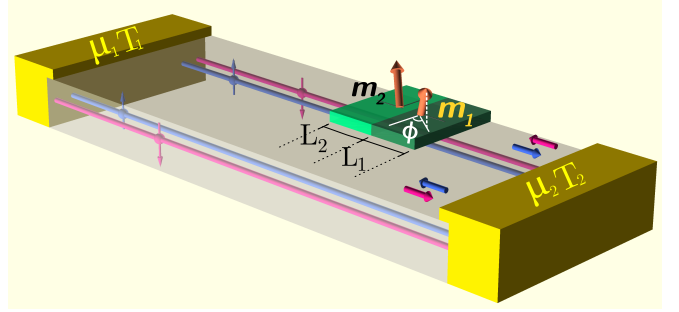


FIG. 1. Sketch of the setup scheme. 2D TI contacted to ohmic contacts at which a bias voltage $eV = \mu_1 - \mu_2$ and temperature difference $\Delta T = T_2 - T_1$ are applied. Two nanomagnets with magnetic moments \mathbf{m}_1 and \mathbf{m}_2 and lengths L_1 and L_2 , are contacted to a helical Kramer's pair of edge states.

ularly promising [54–58]. On another hand, electrical *power generation* out of heat is the aim of thermoelectric heat engines. This is optimized by transmission functions behaving like Heaviside-theta functions within the relevant transport window [52, 53]. In the case of quantum-Hall edge states, configurations with several quantum point contacts and quantum capacitors, have been recently proposed to engineer the transmission function for optimal thermoelectricity by recourse to quantum interference [20].

In the present work we analyze a mechanism for edge-state thermoelectricity in a QSH structure, which does not rely on quantum point contacts not quantum dots. It is based on the coupling of a Kramers pair of helical edge states of the QSH to a magnetic domain. The structure we analyze is sketched in Fig.1, an edge-state pair of a 2D TI is contacted by nanomagnets. We consider two configurations, a single magnetic island with a given magnetic orientation, as well as two attached islands with different orientations of the magnetic moments. In both configurations, the key ingredient is a finite component of the magnetic moments perpendicular to the direction of the spin-orbit interaction of the TI. A similar structure was previously considered in Refs. 59–61, focus-

ing on the interplay between spin-torque induced current and the consequent pumping induced by the precession of the magnetic moment. In combination to superconducting contacts, this structure has been investigated as a platform to realize topological superconductivity [62–64]. Here, we show that the simple two-terminal setup of Fig.1, under the effect of a simultaneous voltage and temperature biases, has the desired properties for optimal heat to electrical work dc conversion. We analyze the transmission function for this structure and the impact of the different features on the thermoelectric response. Remarkably, this function takes the best of the two worlds regarding power generation and large figure of merit, since it has features alike a theta function and delta-function type resonances due to bound states in the gap, as well as peaks alike quantum dots. We provide estimates for the different components of the device and we argue that it is within the present state of the art of fabrication of 2D TI structures [34–36].

Thermoelectric performance in the quantum coherent regime. We briefly review the linear-response thermoelectric approach assuming small differences of chemical potential $eV = \mu_1 - \mu_2$ (with $\mu_1 = \mu$), and temperature $\Delta T = T_2 - T_1$ (with $T_1 = T$), applied at the contacts of the edge states, as indicated in Fig. 1 [2]. The induced charge and heat currents are

$$\begin{pmatrix} I^C/e \\ I^Q \end{pmatrix} = \begin{pmatrix} \mathcal{L}_{11} & \mathcal{L}_{12} \\ \mathcal{L}_{21} & \mathcal{L}_{22} \end{pmatrix} \begin{pmatrix} X_1 \\ X_2 \end{pmatrix}. \quad (1)$$

We have introduced the affinities $X_1 = eV/k_B T$ and $X_2 = \Delta T/k_B T^2$. In the quantum coherent regime, the elements of the Onsager matrix are fully determined by the transmission function $\mathcal{T}(\varepsilon)$ as follows,

$$\mathcal{L}_{ij} = -T \int \frac{d\varepsilon}{h} \frac{\partial f(\varepsilon)}{\partial \varepsilon} (\varepsilon - \mu)^{i+j-2} \mathcal{T}(\varepsilon), \quad (2)$$

where $f(\varepsilon) = 1/(e^{(\varepsilon - \mu)/k_B T} + 1)$. The key for the thermoelectric heat to work conversion is encoded in the off-diagonal coefficient $\mathcal{L}_{12} = \mathcal{L}_{21}$. The quality of this conversion is evaluated in terms of the efficiency (for the heat engine), $\eta^{\text{he}} = (I^C T X_1)/I^Q$, being $P = I^C T X_1$ the generated power, or coefficient of performance (for the refrigerator), $\eta^{\text{fri}} = -I^Q/I^C T X_1$, being $-I^Q$ the heat current extracted from the cold reservoir. In both cases, for a given difference of temperature, the maximum values for these coefficients can be parametrized by the figure of merit $ZT = \mathcal{L}_{21}^2/\text{Det}\hat{\mathcal{L}}$, as follows

$$\eta^{\text{max}} = \eta_C^{\text{he/fri}} \frac{\sqrt{ZT+1} - 1}{\sqrt{ZT+1} + 1}, \quad (3)$$

being $\eta_C^{\text{he}} = [\eta_C^{\text{fri}}]^{-1} = \Delta T/T$ the Carnot efficiency, which is achieved for $ZT \rightarrow \infty$, while the value $\eta^{\text{he/fri}} \sim 0.3 \eta_C$ corresponds to $ZT \sim 3$. As originally shown by Mahan and Sofo, the ideal upper bound $\eta_C^{\text{he/fri}}$ is obtained for $\mathcal{T}(\varepsilon) \sim \delta(\varepsilon - \varepsilon_0)$, while ZT attains high values

when $\mathcal{T}(\varepsilon)$ has peaks within the relevant transport window $|\varepsilon - \varepsilon_0| \sim k_B T$. On another hand, for the heat engine operational mode, the maximum achievable power for a given ΔT and the corresponding efficiency are

$$P_{\text{max}} = \eta_C \frac{\mathcal{L}_{12}^2 X_2}{4\mathcal{L}_{11}}, \quad \eta(P_{\text{max}}) = \eta_C \frac{ZT}{2(ZT+2)}. \quad (4)$$

It has been shown that the maximum power is bounded by $0.32P_0$ for a transmission function of the form $\mathcal{T}(\varepsilon) \sim \theta(\varepsilon - \mu - \varepsilon_0)$, where $P_0 = (k_B \Delta T)^2/h$ [52].

Transmission function. The structure sketched in Fig.1 is modeled by the following Hamiltonian

$$H = \int dx \Psi^\dagger(x) [(-i\hbar v_F \partial_x) \hat{\sigma}_z + J \mathbf{m}(x) \cdot \hat{\sigma}] \Psi(x), \quad (5)$$

where $\Psi(x) = (\psi_{R,\uparrow}(x), \psi_{L,\downarrow}(x))^T$, represent the right(left)-moving electrons with velocity v_F and \uparrow (\downarrow) spin orientations, J is the magnetic exchange interaction between the magnetic moment of the island and the spin of the electrons, and $\hat{\sigma} = (\hat{\sigma}_x, \hat{\sigma}_y, \hat{\sigma}_z)$ are the Pauli matrices. The magnetic island is described by the following piece-wise spacial distribution of the magnetic moment within segments of lengths $L_j = x_j - x_{j-1}$, with $x_0 = 0, x_N = L_{\text{Total}}$.

$$\mathbf{m}(x) = \sum_{j=1}^N \theta(x_j - x) \theta(x - x_{j-1}) \mathbf{m}_j. \quad (6)$$

$\mathbf{m}_j = (m_{j\perp} \cos \phi_j, m_{j\perp} \sin \phi_j, m_{j\parallel})$ is the magnetic moment with components $m_{j\parallel}$ (parallel) and $m_{j\perp}$ (perpendicular) with respect to the direction of the spin-orbit interaction of the TI. We focus on a single island ($N = 1$) and two islands $N = 2$ of the same length but with different orientations of the magnetic moment.

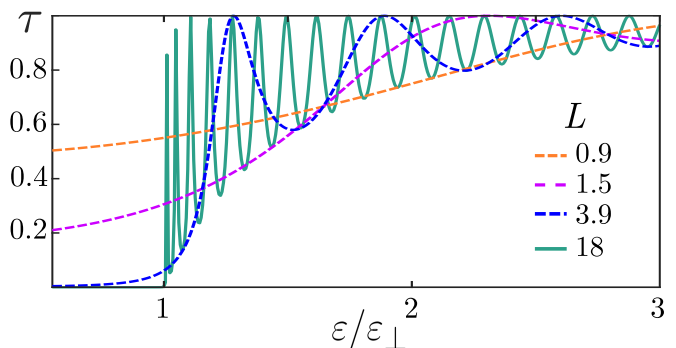


FIG. 2. Transmission function $\mathcal{T}(\varepsilon)$ as a function of the energy within a range of lengths L of an island with an homogeneous magnetic moment. Energies are expressed in units of $\varepsilon_{\perp} = Jm_{\perp}$, lengths are expressed in units of $L_0 = \varepsilon_{\perp}/\hbar v_F$.

In order to calculate the transmission function we proceed as in Ref. [65], starting from the evolution operator in space for the whole scattering region. It reads

$\hat{U}(L, 0) = \prod_{j=1}^N \hat{U}(x_j, x_{j-1})$, with

$$\begin{aligned} \hat{U}(x_j, x_{j-1}) &= \exp\left\{i \frac{\varepsilon_{j\parallel}}{\hbar v_F} L_j\right\} \exp\{-i \boldsymbol{\lambda}_j \cdot \hat{\boldsymbol{\sigma}}\} \\ &= \exp\left\{i \frac{\varepsilon_{j\parallel}}{\hbar v_F} L_j\right\} [\hat{\sigma}_0 \cos \lambda_j - i \mathbf{n}_j \cdot \hat{\boldsymbol{\sigma}} \sin \lambda_j], \end{aligned} \quad (7)$$

being $\boldsymbol{\lambda}_j = (i \varepsilon_{j\perp} \sin \phi_j, -i \varepsilon_{j\perp} \cos \phi_j, \varepsilon) L_j / (\hbar v_F)$, with $\varepsilon_{\parallel, \perp} = J m_{\parallel, \perp}$, and $\mathbf{n}_j = \boldsymbol{\lambda}_j / \lambda_j$. The transmission function is the inverse of the element 2, 2 of the transfer matrix, which is, in turn, the inverse of the matrix $\hat{U}(L, 0)$. Hence, $\mathcal{T}(\varepsilon) = |\text{Det}[\hat{U}(L, 0)] / \mathcal{U}(L, 0)_{1,1}|^2$.

Results for a single homogeneous island. We start by discussing the case of an homogeneous domain, described by the previous Hamiltonian with a single piece, $N = 1$. The resulting transmission function is

$$\mathcal{T}(\varepsilon) = \frac{|\varepsilon_{\perp}^2 - \varepsilon^2|}{|\varepsilon_{\perp}^2 - \varepsilon^2| \cos^2 \lambda + \varepsilon^2 \sin^2 \lambda}, \quad (8)$$

being $\lambda = rL/L_0$, with $L_0 = \hbar v_F / \varepsilon_{\perp}$ and $r = \sqrt{(\varepsilon/\varepsilon_{\perp})^2 - 1}$. Notice that the transmission function does not depend on the detailed orientation of the magnetic moment but only on the projection m_{\perp} perpendicular to the direction of the spin-orbit interaction of the material. It is also symmetrical to $\varepsilon = 0$. The latter introduces an effective coupling between the two Kramer's partners, that may open a gap in the spectrum of magnitude ε_{\perp} .

The behavior of $\mathcal{T}(\varepsilon)$ is illustrated in Fig.2, where we see its dependence on the length of the island. For short islands, there is a sizable tunneling amplitude through the magnetic island, while as the length of the magnet increases, the transmission function tends to a step function close to $\varepsilon \sim \varepsilon_{\perp}$. We get the following behavior of the transmission function at the opening of the gap as a function of length $\mathcal{T}(\varepsilon_{\perp}) = [1 + (L/L_0)^2]^{-1}$, while the slope behaves as $d\mathcal{T}/d\varepsilon|_{\varepsilon_{\perp}} = 2(L/L_0)^4 [1 + (L/L_0)^2] / 3 [1 + (L/L_0)^2]^3$, which saturates at the value of 2/3, for increasing L . For energies $\varepsilon > \varepsilon_{\perp}$, $\mathcal{T}(\varepsilon)$ exhibits oscillations with maxima $\mathcal{T}^{\max}(\varepsilon_n) = 1$ and minima $\mathcal{T}^{\min}(\varepsilon_m) = 1 - (\varepsilon_{\perp}/\varepsilon_m)^2$ at energies satisfying $(\varepsilon_{n(m)})^2 = (\varepsilon_{\perp})^2 + (\pi \alpha_{n(m)} \hbar v_F / L)^2$, with $\alpha_{n(m)}$ being an integer (half-integer) number, respectively.

The impact of the features of the transmission function on the thermoelectric performance for the heat engine is illustrated in Fig.3 for two lengths of the magnetic domain, in a range of chemical potentials close to the edge of the energy gap, within a temperature range scaled by the reference temperature $T_0 = \varepsilon_{\perp}/k_B$. For the shortest length shown in panels (a) and (b), $L = 10L_0$, $\mathcal{T}(\varepsilon_{\perp}) < 0.01$ and $d\mathcal{T}/d\varepsilon|_{\varepsilon_{\perp}} \sim 0.65$, i.e. close to the maximal slope (2/3), implying a pronounced step in the transmission function at the closing of the energy gap. The plots shown in Figs.(c) and (d) correspond to an island of twice the length, and the step is only slightly more pronounced. For very low temperatures, within a scale

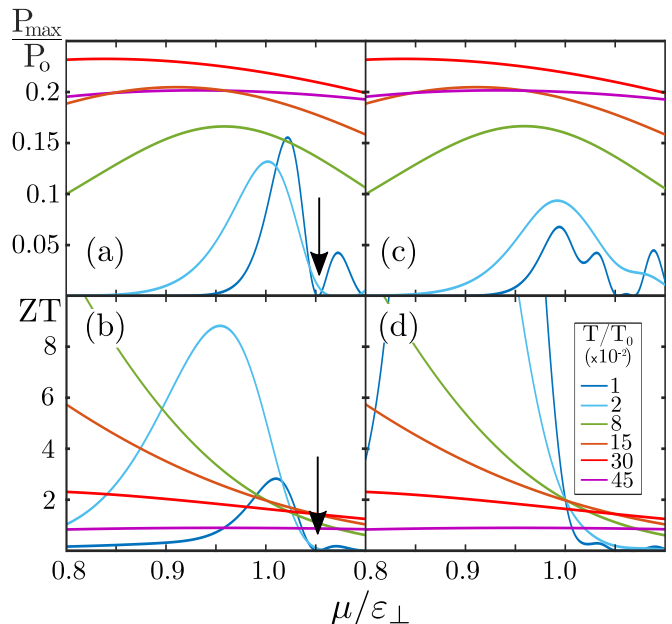


FIG. 3. Maximum power (upper panels) and figure of merit (lower panels) for the case of $L = 10L_0$ (a)-(b) and $L = 20L_0$ (c)-(d). The temperatures are expressed in units of $T_0 = \varepsilon_{\perp}/k_B$ and the power is expressed in units of $P_0 = (k_B \Delta T)^2 / h$. Other details are the same as in Fig.2.

$k_B T$ smaller than the width of the peaks of $\mathcal{T}(\varepsilon)$, both P_{\max} and ZT vanish for $\mu = \varepsilon_n$ (see arrows in panels a. and b.). As the temperature increases, the behavior of these quantities is ruled by the effect of several peaks. At sufficiently high temperature, such that several maxima of $\mathcal{T}(\varepsilon)$ are included in an energy window of width $k_B T$, the behavior is dominated by the average between the envelopes for the minima and the maxima of $\mathcal{T}(\varepsilon)$. The resulting function is approximately a smoothed step-function, independently of the length of the island. For this reason, P_{\max} shows a wide maximum centered at $\sim |\varepsilon_{\perp} - \mu| \sim k_B T$ [20, 52]. The maximum is as high as $\sim 0.28P_0$, i.e. $\sim 87\%$ of the bound $0.32P_0$. $\mathcal{T}(\varepsilon)$ is symmetric with respect to $\varepsilon = 0$ and has a well-function of unit depth and width $\sim 2\varepsilon_{\perp}$. This feature dominates the behavior of the power and ZT at high temperatures. These properties depend mildly on the length of the island. Details of the effect of the different features of $\mathcal{T}(\varepsilon)$ on the thermoelectric response as a function of T are presented in the supplementary material (SM) [66].

Results for two domains. We now turn to analyze the effect of having an inhomogeneous magnetization along the island. We focus on the simple case where we have two pieces, corresponding to $N = 2$ in Eq.(7) with $L_1 = L_2 = L$, $\phi_1 = 0$, $\phi_2 = \phi$, and $\varepsilon_{\perp,1} = \varepsilon_{\perp,2} = \varepsilon_{\perp}$. The resulting

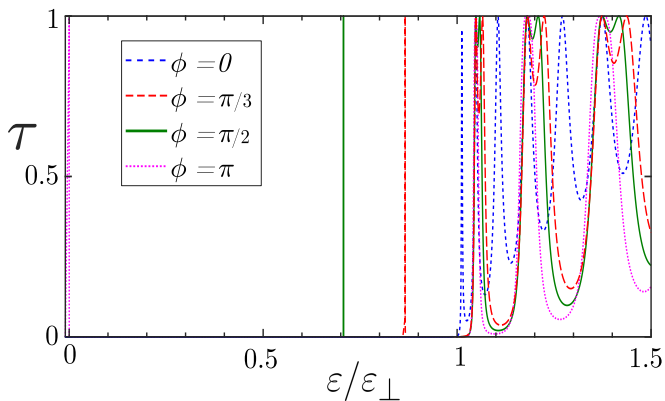


FIG. 4. Transmission function \mathcal{T} for two magnetic domains of equal size ($L = 10L_0$) for several angles ϕ .

transmission function reads,

$$\mathcal{T}(\varepsilon) = \left\{ \left[\cos^2 \lambda + \frac{\sin^2 \lambda}{r^2} \left(\cos \phi - \frac{\varepsilon^2}{\varepsilon_{\perp}^2} \right) \right]^2 + \left[-\frac{\varepsilon}{\varepsilon_{\perp}} \frac{\sin 2\lambda}{r} + \sin \phi \frac{\sin^2 \lambda}{r^2} \right]^2 \right\}^{-1}. \quad (9)$$

For the case of an antiferromagnetic configuration ($\phi = \pi$), there is a simple expression for the minima. It reads $\mathcal{T}^{min}(\varepsilon_m) = \left[(\varepsilon_m^2 - \varepsilon_{\perp}^2) / (\varepsilon_m^2 + \varepsilon_{\perp}^2) \right]^2$, where ε_m has the same expression as before. The new feature in the present case, in comparison to the case of a single magnetic moment, is the existence of resonances within the gap, $|\varepsilon| < \varepsilon_{\perp}$, for $\phi \neq 0$. For $\phi = \pi$, we can verify analytically the existence of a resonance at $\varepsilon = 0$ [66].

The transmission function is shown in Fig. 4 for a set of orientations. The corresponding thermoelectric response is shown in 5. Close to the edge of the gap, the minima of $\mathcal{T}(\varepsilon)$ for antiferromagnetic alignment, are deeper than the ones for a single ferromagnetic island. On the other hand, for $\phi = \pi$, the energy difference between peaks is twice the one for $\phi = 0$ (notice that the latter corresponds to a single island with total length $2L$). Hence, for two antiferromagnetic domains, the first peak after the closing of the gap is expected to show a thermoelectric response with a high figure of merit, similar to that of a Lorentzian function within a range of temperatures larger than in the case of a single ferromagnetic one. This is also the case of the resonances within the gap, as shown in Fig. 5. See more details in Ref. [66].

Conclusions. We have analyzed the transmission function characterizing the coherent transport of electrons in a structure consistent of a pair of helical edge states of a 2D TI coupled by a magnetic island with a magnetic moment having a component perpendicular to the direction of the spin orbit of the TI. We have shown that this setup has the necessary conditions to achieve high performance thermoelectricity. The key is the opening of

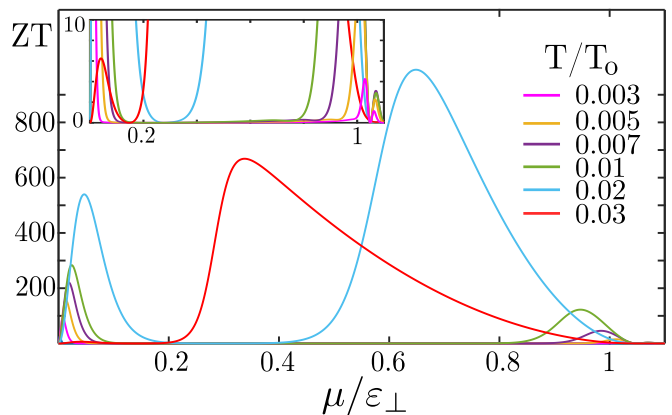


FIG. 5. Figure of merit ZT for two magnetic domains of length $L = 10L_0$ with antiferromagnetic alignment of the magnetic moments. The inset corresponds to a zoom in the range $ZT < 10$. Other details are similar to previous figures.

a gap in the spectrum of the helical edges with a steep increase of the transmission function at the opening of the propagating modes in the spectrum. Depending on the energy range and the configuration of the magnetic domains, the transmission function has features akin to a theta-function, as well as with features akin to a delta-function, which are known to be optimal for high-power production and figure of merit, respectively. Due to the resonant states in the gap for two magnetic domains, very large values of the figure of merit, $ZT > 100$, are attained for the heat-engine and refrigeration modes. Our calculations focus on a single pair of edge states, but the currents simply scale in a factor two when the pair at the opposite edge is considered. The range of operation is set by the magnetic gap ε_{\perp} . For a single magnetic moment with $\mu_{BM} \sim 1.8 - 4T$ [67], we estimate $\varepsilon_{\perp} \sim 1 - 2 \times 10^{-4} eV$, corresponding to reference temperatures $T_0 \sim 1.2 - 2.4 K$. According to our study, the device operates as a heat engine at a high performance (larger than 85% of the optimal bound) regarding power generation with a figure of merit $ZT \gg 1$ for $T < 0.5T_0$ with a length of the magnetic island of $\sim 10L_0$, being $L_0 = \varepsilon_{\perp} / \hbar v_F$. Taking estimates for the Fermi velocity of the helical edge states in quantum wells of HgTe from Ref. [34], we have $\hbar v_F \sim 0.9 eV/nm$, leading to $L_0 \sim 10 - 20 \mu m$. These parameters are at the state of the art of present experimental realizations.

Acknowledgements. We thank A. Aligia and P. Roura-Bas for carefully reading our manuscript and useful comments. We acknowledge support from CONICET, Argentina. We are sponsored by PIP-RD 20141216-4905 of CONICET, PICT-2014-2049 and PICT-2017-2726 from Argentina, as well as the Alexander von Humboldt Foundation, Germany (LA).

SUPPLEMENTAL MATERIAL: OPTIMAL THERMOELECTRICITY WITH QUANTUM SPIN-HALL EDGE STATES

In order to gain insight on the features of the transmission function $\mathcal{T}(\varepsilon)$ ruling the thermoelectric response of a single Kramer's pair of helical edge states of the QSH coupled to a nanomagnet, we analyze simpler functions and take them as a reference. In particular, we analyze the thermoelectric response of Lorentzian (Sec. A A), Heaviside-step (Sec. A B) and well-shaped (Sec. A C) transmission functions. At different energy scales, $\mathcal{T}(\varepsilon)$ for the nanomagnet-QSH system contains ingredients of these three functions, which become dominant depending on the temperature range. We also show the existence of a resonant state in the case of two magnetic domains arranged in an antiferromagnetic configuration Sec. C.

Appendix A THERMOELECTRIC PERFORMANCE OF REFERENCE FUNCTIONS

A Lorentzian-function

We consider a transmission function composed by M Lorentzians:

$$\mathcal{T}(\varepsilon) = \sum_{i=1}^M \frac{\gamma_i^2}{\gamma_i^2 + (\varepsilon_i - \varepsilon)^2}. \quad (10)$$

We focus on $M = 3$ with widths γ_i and centers ε_i chosen to reproduce the three oscillations after the closing of the gap of the transmission function of the nanomagnet-QSH system with $L/L_0 = 10$. The evolution of the corresponding ZT and P_{\max} as functions of T is shown in Fig. 6. For temperatures lower than the width and distance between peaks, each peak behaves like a single independent Lorentzian-transmission. Under this regime, both ZT and power are increasing functions of T .

As the temperature increases and $k_B T$ becomes of the order of magnitude of the energy difference between maxima, the response of the different peaks is averaged. This regime is analyzed in Fig. 7. ZT remains an increasing function of the temperature, having a single effective peak centered in the middle of the three Lorentzians. However, P_{\max} turns to be a decreasing function of T .

B Heaviside-function

Now we turn to review P_{\max} and ZT for the case of a transmission function of the form $\mathcal{T}(\varepsilon) = \theta(\varepsilon - \varepsilon_0)$, a Heaviside function. Results are shown in Fig. 8. For wide range of temperatures, the maximum achievable power, $0.32P_0$, where $P_0 = (k_B \Delta T)^2/h$, is reached [51, 52] at $\mu \sim -k_B T$. Instead, ZT is a decreasing function of the temperature, and drops very rapidly to $ZT \sim 0$ in the region of $\mu > \varepsilon_0$, where $\mathcal{T} = 1$.

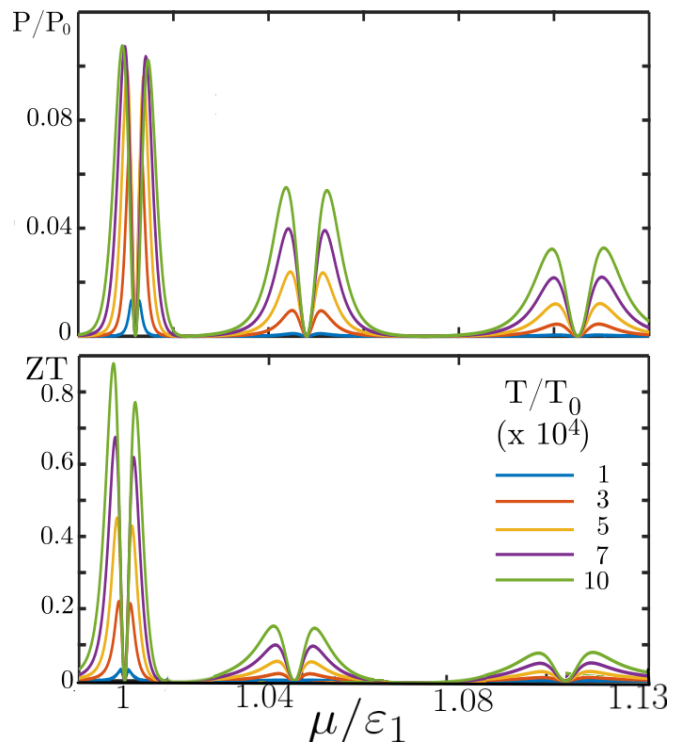


FIG. 6. Maximum power and ZT for the Lorentzian model within the low-temperature regime where each Lorentz function is solved. Parameters used are $\varepsilon_2 = 1.035\varepsilon_1$, $\varepsilon_3 = 1.038\varepsilon_1$, $\gamma_1 = 9.8 \times 10^{-4} \varepsilon_1$, $\gamma_2 = 3.9 \times 10^{-3} \varepsilon_1$ and $\gamma_3 = 5.9 \times 10^{-3} \varepsilon_1$.

C Well-shaped function

Finally, we consider a well-shaped function of unit depth of the form $\mathcal{T}(\varepsilon) = \theta(\varepsilon - \varepsilon_0) + \theta(-\varepsilon - \varepsilon_0)$, alike the gap of the transmission function of the nanomagnet coupled to the helical edge states. Results are shown in Fig. 9. For low temperatures, this function leads to a thermoelectric performance with the maximum achievable power $P_{\max} = 0.32P_0$. The behavior of both power and ZT is similar to that of two separated Heaviside-type transmission functions. For $k_B T > 0.1\varepsilon_{\perp}$, the behavior these quantities changes and they decrease with T , presenting maxima close to the edge of the steps.

Appendix B THERMOELECTRIC REGIMES OF THE NANOMAGNET COUPLED TO THE HELICAL EDGE STATES

Given the previous discussion we can expect three regimes as a function of the temperature in the thermoelectric behavior of the system under investigation, which has a transmission function with ingredients of the three functions described in the previous section. Concretely, we expect that at low temperatures, where resonances and peaks are resolved, the thermoelectric response resembles that of the Lorentzian function, at higher tem-

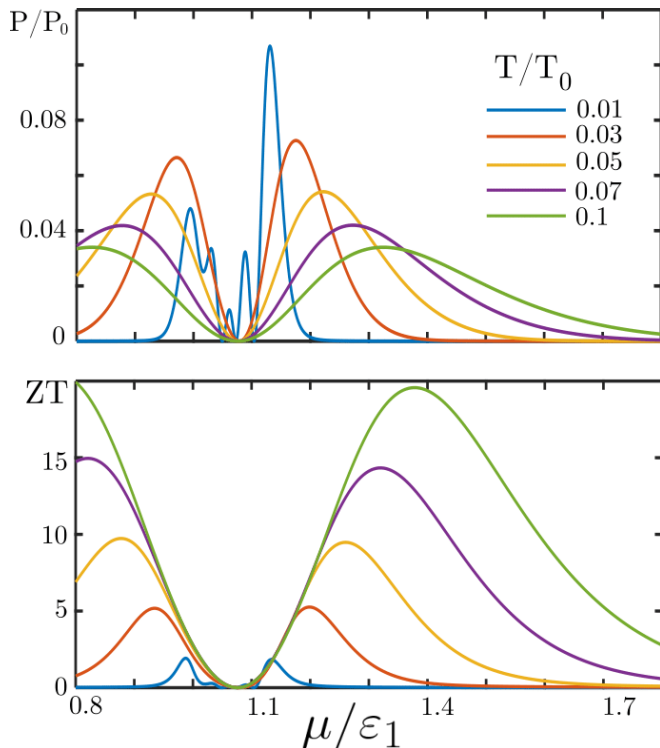


FIG. 7. Maximum power and ZT for the Lorentzian model within the temperature regime with $k_B T$ larger than the separation between maxima.

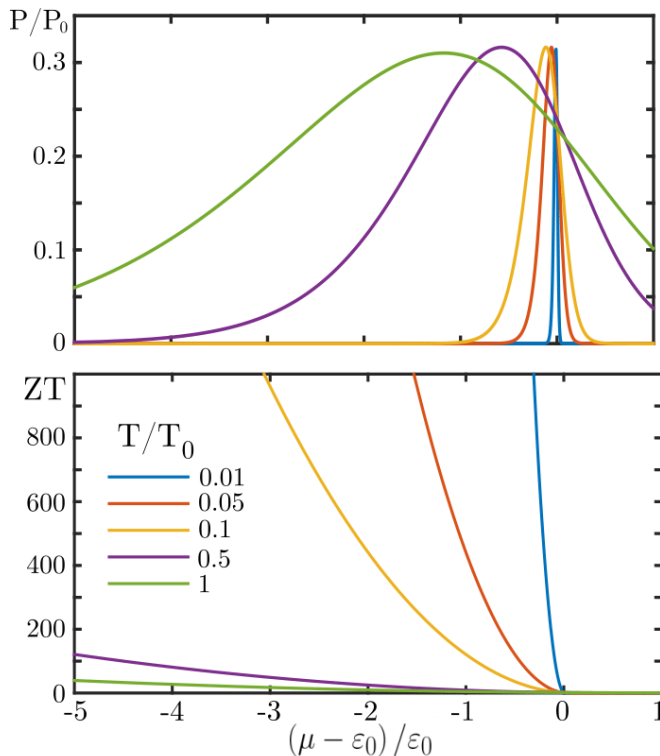


FIG. 8. Maximum power and ZT for Heaviside step function for several temperatures.

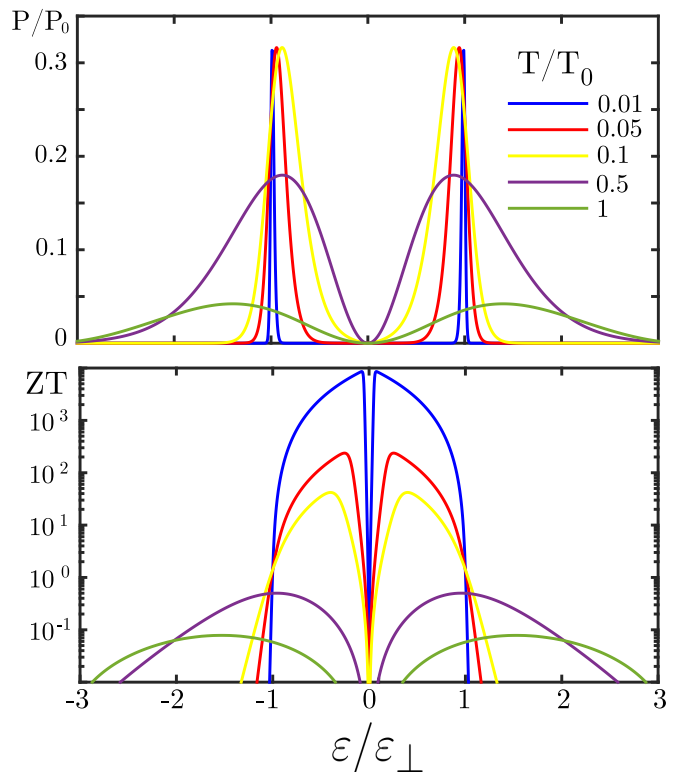


FIG. 9. Power and ZT for a well-function as function of $\epsilon/\epsilon_{\perp}$ for several temperatures. At low temperatures it reaches the maximum achievable power, $P_{\max} = 0.32P_0$, near the edge of the gap. For higher temperatures it drops zero. For ZT at low temperatures it becomes very great but as temperature increases it falls several orders of magnitude.

peratures, the behavior of the Heaviside function becomes dominant and at even higher temperatures, the well-shape due to the gap causes the decreasing behavior of both P_{\max} and ZT as functions of T for all values of the chemical potential μ .

An overview of the two lowest-energy regimes is presented in Fig. 10. Here, we show the functions $\overline{ZT} = \text{Max}_{\mu} [ZT]$ and $\overline{P_{\max}} = \text{Max}_{\mu} [P_{\max}]$, where Max_{μ} denotes the maximum value of the quantity over the whole range of values of μ . The boundary for the lowest-temperature regime is identified with the range of T below the one corresponding to the minimum of $[P_{\max}]$. This regime is akin to the Lorentzian-type response and is non-universal, since it depends on the details of the peaks of $\mathcal{T}(\epsilon)$. The latter are determined by the length of the island and the number of domains. In the case of two antiferromagnetic domains, it is possible to distinguish a narrow feature, which is associated to the resonance within the gap, followed by a second feature, which is associated to the the first peak after the closing of the gap. For islands with a single domain, we can distinguish only one feature, which is associated to the first peak after the closing of the gap. For larger temperatures, we enter the regime dominated by the Heaviside-type function corresponding to averaging the envelopes of the minima

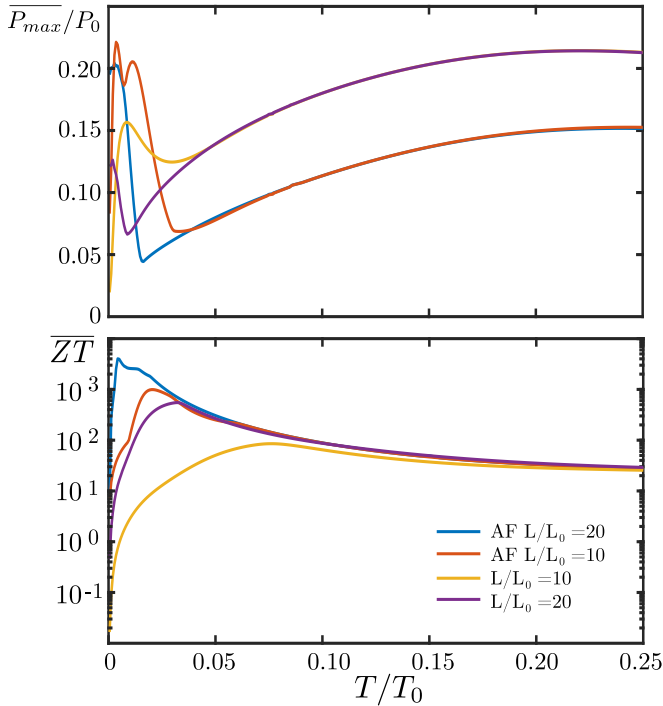


FIG. 10. $\overline{ZT} = \text{Max}_\mu [ZT]$ and $\overline{P_{\max}} = \text{Max}_\mu [P_{\max}]$, corresponding to the maximum values of P_{\max} and ZT over the whole range of μ , as functions of the temperature T . AF denotes islands with two domains antiferromagnetically aligned.

and maxima of the transmission function for $\varepsilon > \varepsilon_\perp$. While the maxima correspond to $\mathcal{T} = 1$, the minima are deeper for two antiferromagnetic domains than for a single domain. Hence, the values of $\text{Max}_\mu [P_{\max}]$ within this regime are higher for a single domain than for two antiferromagnetic ones. For both orientations, the behavior is universal, in the sense that it does not depend on the length of the island. The figure shows the onset

of the third (high-temperature) regime, where the well-shape becomes dominant and $\text{Max}_\mu [P_{\max}]$ turns to be a decreasing function of T .

Appendix C RESONANT STATE IN ANTIFERROMAGNETIC CONFIGURATION

The inverse of transmission function of two magnetic domains with length L and a relative orientation ϕ of the component of the magnetization perpendicular to the spin-orbit interaction of the TI, takes the following simple form

$$[\mathcal{T}(\varepsilon, l, \phi)]^{-1} = \left[\cos^2 \lambda + \frac{\sin^2 \lambda}{r^2} (\cos \phi - x^2) \right]^2 + \left[-x \frac{\sin 2\lambda}{r} + \sin \phi \frac{\sin^2 \lambda}{r^2} \right]^2, \quad (11)$$

where $l = L/L_0$, $x = \varepsilon/\varepsilon_\perp$, $r = \sqrt{x^2 - 1}$ and $\lambda = lr$. We see that for $\varepsilon = 0$, the latter function reads

$$\begin{aligned} [\mathcal{T}(0, l, \phi)]^{-1} &= \left(\cos^2(li) + \left(\frac{\sin li}{i} \right)^2 \right) + \left(\sin \phi \left(\frac{\sin li}{i} \right)^2 \right)^2 \\ &= \left(\cosh^2 l + \sinh^2 l \cos \phi \right)^2 + \sin^2 \phi \sinh^2 l \\ &= \left(1 + (1 + \cos \phi) \sinh^2 l \right)^2 + \sin^2 \phi \sinh^2 l, \end{aligned} \quad (12)$$

where we see that $\mathcal{T}(0, l, \phi) \sim 0$ for $L > L_0$ except for $\phi = (2n+1)\pi$, with n integer, in which case $\mathcal{T}(0, l, (2n+1)\pi) = 1$. Therefore, we conclude that for $\phi = (2n+1)\pi$, there is a resonant state in the center of the gap, with energy $\varepsilon = 0$. The width of this resonant state depends on e^{-l} , which means that the width of the resonance decreases with l .

-
- [1] F. Giazotto, F., T. T. Heikkilä, A. Luukanen, A. M. Savin, and J.P. Pekola, Opportunities for mesoscopies in thermometry and refrigeration: Physics and applications. *Rev. Mod. Phys.* **78** 2172006 (2006).
- [2] G. Benenti, G. Casati, K. Saito, R. S. Whitney, Fundamental aspects of steady-state conversion of heat to work at the nanoscale, *Phys. Rep.* **694**, 1 (2017).
- [3] J. P. Eisenstein and J. L. Reno, Observation of Chiral Heat Transport in the Quantum Hall Regime, G. Granger, *Phys. Rev. Lett.* **102**, 086803 (2009).
- [4] S. G. Nam, E. H. Hwang and H. J. Lee, Thermoelectric detection of chiral heat transport in graphene in the quantum Hall regime, *Phys. Rev. Lett.* **110** 22680 (2013).
- [5] L. Arrachea and E. Fradkin, Chiral heat transport in driven quantum Hall and quantum spin Hall edge states, *Phys. Rev. B* **84**, 235436 (2011).
- [6] S. Jezouin, F D. Parmentier, A. Anthore, U. Gennser, A. J. Cavanna and F. Pierre, Quantum limit of heat flow across a single electronic channel, *Science* **342** 601 (2013).
- [7] A. Cappelli, M. Huerta, and G. Zemba, Thermal Transport in Chiral Conformal Theories and Hierarchical Quantum Hall States, *Nucl. Phys. B* **636**, 568 (2002).
- [8] E. Grosfeld and S. Das, Probing the Neutral Edge Modes in Transport across a Point Contact via Thermal Effects in the Read-Rezayi Non-Abelian Quantum Hall States, *Phys. Rev. Lett.* **102**, 106403 (2009).
- [9] T. Karzig, G. Refael, L. I. Glazman, F. von Oppen, Energy Partitioning of Tunneling Currents into Luttinger Liquids, *Phys. Rev. Lett.* **107**, 176403 (2011).
- [10] H. Aita, L. Arrachea, C. Naón, and E. Fradkin, Heat transport through quantum Hall edge states: Tunneling versus capacitive coupling to reservoirs, *Phys. Rev. B* **88**, 085122 (2013).
- [11] G. Viola, S. Das, E. Grosfeld, and A. Stern, Thermoelectric probe for neutral edge modes in the fractional quantum Hall regime, *Phys. Rev. Lett.* **109**, 146801 (2012).

- [12] I. Gurman, R. Sabo, M. Heiblum, V. Umansky, and D. Mahalu, Extracting net current from an upstream neutral mode in the fractional quantum Hall regime, *Nature Comm.* **3**, 1289 (2012).
- [13] C. Altimiras, H. le Sueur, U. Gennser, A. Cavanna, D. Mailly and F. Pierre, Tuning energy relaxation along quantum Hall channels, *Phys. Rev. Lett.* **105**, 226804 (2010).
- [14] V. Venkatachalam, S. Hart, L. Pfeiffer, K. West, and A. Yacoby, Local thermometry of neutral modes on the quantum Hall edge *Nature Physics* **8**, 676 (2012).
- [15] A. Cavanna, D. Mailly, and F. Pierre, Chargeless Heat Transport in the Fractional Quantum Hall Regime, C. Altimiras, H. le Sueur, U. Gennser, A. Anthore, *Phys. Rev. Lett.* **109**, 026803 (2012).
- [16] M. Banerjee, M. Heiblum, A. Rosenblatt, Y. Oreg, D. E. Feldman, A. Stern, and V. Umansky, Observed quantization of anyonic heat flow, *Nature* **545**, 75 (2017).
- [17] Theory of Disorder-Induced Half-Integer Thermal Hall Conductance D. F. Mross, Y. Oreg, A. Stern, G. Margalit, M. Heiblum, *Phys. Rev. Lett.* **121**, 026801 (2018).
- [18] A. Aharon, Y. Oreg, A. Stern, Phenomenological theory of heat transport in the fractional quantum Hall effect, *Phys. Rev. B* **99**, 041302 (2019).
- [19] R. Sánchez, B. Sothmann, A. N. Jordan, Chiral thermoelectrics with quantum Hall edge states, *Phys. Rev. Lett.* **114**, 146801 (2015).
- [20] P. Samuelsson, S. Kheradsoud, B. Sothmann Optimal quantum interference thermoelectric heat engine with edge states, *Phys. Rev. Lett.* **118**, 256801 (2017).
- [21] L. Vannucci, F. Ronetti, G. Dolcetto, M. Carrega, M. Sasseti, Interference-induced thermoelectric switching and heat rectification in quantum Hall junctions *Phys. Rev. B* **92**, 075446 (2015).
- [22] P. Roura-Bas, L. Arrachea, E. Fradkin, Enhanced thermoelectric response in the fractional quantum Hall effect *Phys. Rev. B* **97**, 081104 (2018).
- [23] A Xiao-Qin Yu, Zhen-Gang Zhu, Gang Su, A. -P. Jauho, spin caloritronic battery, *Phys. Rev. Applied* **8**, 054038 (2017).
- [24] Flavio Ronetti, Luca Vannucci, Giacomo Dolcetto, Matteo Carrega, Maura Sasseti, Spin-thermoelectric transport induced by interactions and spin-flip processes in two dimensional topological insulators, *Phys. Rev. B* **93**, 165414 (2016).
- [25] Sun-Yong Hwang, Rosa Lopez, Minchul Lee, David Sanchez, Nonlinear spin-thermoelectric transport in two-dimensional topological insulators, *Phys. Rev. B* **90**, 115301 (2014).
- [26] Po-Hao Chang, Mohammad Saeed Bahramy, Naoto Nagaosa, Branislav K. Nikolic Giant thermoelectric effect in graphene-based topological insulators with nanopores, *Nano Lett.* **14**, 3779 (2014).
- [27] D. G. Rothe, E. M. Hankiewicz, B. Trauzettel, M. Guigou, Spin-dependent thermoelectric transport in HgTe/CdTe quantum wells, *Phys. Rev. B* **86**, 165434 (2012).
- [28] P. Roura-Bas, L. Arrachea, and E. Fradkin, Helical spin thermoelectrics controlled by a side-coupled magnetic quantum dot in the quantum spin Hall state, *Phys. Rev. B* **98**, 195429 (2018).
- [29] D. Sanchez, R. Sanchez, R. Lopez, B. Sothmann, Nonlinear chiral refrigerators, arXiv:1904.04506.
- [30] Arjun Mani, Colin Benjamin, Helical thermoelectrics and refrigeration, *Phys. Rev. E* **97**, 022114 (2018).
- [31] C. L. Kane and E. J. Mele, Z_2 Topological Order and the Quantum Spin Hall Effect, *Phys. Rev. Lett.* **95**, 146802 (2005).
- [32] C. L. Kane and E. J. Mele, Quantum Spin Hall Effect in Graphene, *Phys. Rev. Lett.* **95**, 226801 (2005).
- [33] B. A. Bernevig, T. L. Hughes, and S.-C. Zhang, Quantum Spin Hall Effect and Topological Phase Transition in HgTe Quantum Wells, *Science* **314**, 1757 (2006).
- [34] M. König, S. Wiedmann, C. Brüne, A. Roth, H. Buhmann, L. W. Molenkamp, X. L. Qi, and S.-C. Zhang, Quantum Spin Hall Insulator State in HgTe Quantum Wells, *Science* **318**, 766 (2007).
- [35] A. Roth, C. Brüne, H. Buhmann, L. W. Molenkamp, J. Maciejko, X-L. Q, S-C Zhang, Nonlocal Transport in the Quantum Spin Hall State *Science* **325**, 294 (2009).
- [36] C. Brüne, A. Roth, H. Buhmann, E. M. Hankiewicz, L. W. Molenkamp, J. Maciejko, X-L. Qi, and S-C. Zhang, Spin polarization of the quantum spin Hall edge states *Nature Phys.* **8**, 485 (2012).
- [37] B. J. van Wees, H. van Houten, C. W. J. Beenakker, J. G. Williamson, L. P. Kouwenhoven, D. van der Marel, C. T. Foxon, Quantized conductance of point contacts in a two-dimensional electron gas. *Phys. Rev. Lett.* **60**, 848 (1988).
- [38] H. van Houten, L. W. Molenkamp, C. W. J. Beenakker, C.T. Foxon, Thermoelectric properties of quantum point contacts. *Semicond. Sci. Technol.* **7**, B215 (1992).
- [39] M. Büttiker, Quantized transmission of a saddle-point constriction. *Phys. Rev. B* **41**, 7906 (1990).
- [40] F. Dolcini, Full electrical control of charge and spin conductance through interferometry of edge states in topological insulators, *Phys. Rev. B* **83**, (2011).
- [41] P. Virtanen, P. Recher, Dephasing of spin and charge interference in helical Luttinger liquids, *Phys. Rev. B* **83**, 115332 (2011)
- [42] F. Romeo, R. Citro, D. Ferraro and M. Sasseti, Electrical switching and interferometry of massive Dirac particles in topological insulator constrictions, *Phys. Rev. B* **86**, 165418 (2012).
- [43] B. Rizzo, L. Arrachea, M. Moskalets, Transport phenomena in helical edge states interferometers. A Green's function approach, *Phys Rev B* **88**, 155433 (2013).
- [44] F. Crépin, J. C. Budich, F. Dolcini, P. Recher, and B. Trauzettel, Renormalization group approach for the scattering off a single Rashba impurity in a helical liquid, *Phys. Rev. B* **86**, 121106 (R) (2012).
- [45] G. Dolcetto, F. Cavaliere, D. Ferraro, and M. Sasseti, Generating and controlling spin-polarized currents induced by a quantum spin Hall antidot, *Phys. Rev. B* **87**, 085425 (2013).
- [46] K. T. Law, C. Y. Seng, Patrick A. Lee, and T. K. Ng, Quantum dot in a two-dimensional topological insulator: The two-channel Kondo fixed point *Phys. Rev. B* **81**, 041305 (2010).
- [47] T. Posske, C-X Liu, J. C. Budich, and B. Trauzettel, Exact Results for the Kondo Screening Cloud of Two Helical Liquids, *Phys. Rev. Lett.* **110**, 016602 (2013).
- [48] B. Probst, P. Virtanen, P. Recher, Controlling spin polarization of a quantum dot via a helical edge state, *Phys. Rev. B* **92**, 045430 (2015).
- [49] B. Rizzo, A. Camjayi, Liliana Arrachea Transport in quantum spin Hall edges in contact to a quantum dot *Phys. Rev. B* **94**, 125425 (2016).

- [50] G. D. Mahan, J. O. Sofo, The best thermoelectric. Proc. Natl. Acad. Sci. U.S.A. **93**, 7436 (1996).
- [51] G. Benenti, K. Saito, and G. Casati, Thermodynamic Bounds on Efficiency for Systems with Broken Time-Reversal Symmetry, Phys. Rev. Lett. **106**, 230602 (2011).
- [52] R. S. Whitney, Most Efficient Quantum Thermoelectric at Finite Power Output. Phys. Rev. Lett. **112**, 130601 (2014) .
- [53] R. S. Whitney, Finding the quantum thermoelectric with maximal efficiency and minimal entropy production at given power output, Phys. Rev. B **91**, 115425 (2015).
- [54] M. Josefsson, A. Svilans, A. M. Burke, E. A. Hoffmann, S. Fahlvik, C. Thelander, M. Leijnse, H. Linke, A quantum-dot heat engine operating close to the thermodynamic efficiency limits, Nat. Nanotechnol. **13**, 920 (2018).
- [55] P. A. Erdman, F. Mazza, R. Bosisio, G. Benenti, R. Fazio, Fabio Taddei Thermoelectric properties of an interacting quantum dot-based heat engine Phys. Rev. B **95**, 245432 (2017).
- [56] D. Prete, Paolo A. Erdman, V. Demontis, V. Zannier, D. Ercolani, L. Sorba, F. Beltram, F. Rossella, F. Taddei, S. Roddaro, Thermoelectric conversion at 30K in InAs/InP nanowire quantum dots, arXiv:1903.06935.
- [57] B. Dutta, J. T. Peltonen, D. S. Antonenko, M. Meschke, M. A. Skvortsov, B. Kubala, J. König, C. B. Winkelmann, H. Courtois, and J. P. Pekola, Thermal Conductance of a Single-Electron Transistor, Phys. Rev. Lett. **119**, 077701 (2017).
- [58] O. Entin-Wohlman, Y. Imry and A. Aharony, Enhanced performance of joint cooling and energy production, Phys. Rev. B **91**, 054302 (2015).
- [59] Q. Meng, S. Vishveshwara, T. L. Hughes, Spin-transfer torque and electric current in helical edge states in quantum spin Hall devices, Phys. Rev. B **90**, 205403 (2014).
- [60] L. Arrachea and F. von Oppen, Nanomagnet coupled to quantum spin Hall edge: An adiabatic quantum motor, Physica E **74**, 596 (2015).
- [61] P. G. Silvestrov, P. Recher, P. W. Brouwer, Noiseless manipulation of helical edge state transport by a quantum magnet, Phys. Rev. B **93**, 205130 (2016).
- [62] L. Fu and C. L. Kane, Josephson current and noise at a superconductor/quantum-spin-Hall-insulator/superconductor junction Phys. Rev. B **79**, 161408 (2009).
- [63] M. Houzet, J. S. Meyer, D. M. Badiane, and L. I. Glazman, Dynamics of Majorana States in a Topological Josephson Junction Phys. Rev. Lett. **111**, 046401 (2013).
- [64] Francois Crépin, Björn Trauzettel, and Fabrizio Dolcini, Signatures of Majorana bound states in transport properties of hybrid structures based on helical liquids, Phys. Rev. B **89**, 205115 (2014).
- [65] R. Bustos-Marun, G. Refael, and F. von Oppen, Adiabatic Quantum Motors, Phys. Rev. Lett. **111**, 060802 (2013).
- [66] See supplementary material for details on the behavior of the maximum power for the heat engine and the figure of merit of reference transmission functions.
- [67] G. Scheunert, O. Heinonen, R. Hardeman, A. Lapicki, M. Gubbins, and R. M. Bowman, A review of high magnetic moment thin films for microscale and nanotechnology applications. Appl. Phys. Rev. **3**, 011301, (2016).